



# Influence of Precipitation Uncertainty and Land Use Change on the Optimal Catchment Scale Configuration of Green Stormwater Infrastructure

Ashish Shrestha<sup>1</sup> and Margaret Garcia, M.ASCE<sup>2</sup>

Abstract: Adoption of green stormwater infrastructure (GSI) as a sustainable stormwater measure to manage urban flooding has gained momentum globally. Modeling and analysis tools are available to guide its design and planning. However, the impact of uncertainty in design precipitation estimates, and change in land use on the optimal configuration of GSI has not yet been assessed. The uncertainty in design precipitation estimates influences the amount and cost of GSI; and urban forms, space availability and existing drainage infrastructure influence the placement and ideal types of GSI. Further, climate change and conversion of pervious to impervious surfaces create varied impacts across cities. In this paper we investigate how such catchment scale optimal configurations of GSI, defined as ideal selection of type, amount and spatial distribution of GSI, vary (1) across uncertainty within design precipitation estimates from NOAA Atlas 14; and (2) with increasing urban imperviousness. We analyze this across two different cases of urban forms: (1) a catchment with mixed use buildings where bioretention (i.e., ground based) and green roofs (i.e., over ground based) are feasible, and (2) a catchment with only residential buildings where only bioretention is feasible. For this aim we utilize the USEPA's stormwater management model (SWMM) to construct onedimensional hydrologic-hydraulic models using stormwater networks of two separate locations in Phoenix, Arizona. We couple the SWMM model with nondominated sorting genetic algorithm (NSGA-II) to develop a multiobjective optimal GSI planning framework to determine amount, type and location for GSI implementation. We found that varying the design precipitation from the lower to upper bound of the confidence interval for NOAA Atlas 14, resulted in a larger difference in the amount of GSI required than the effect of land use change from 2001 to 2019. This highlights the important of accurate design storm estimates and the value of modular GSI in adapting stormwater systems under uncertainty. DOI: 10.1061/JSWBAY.SWENG-471. © 2023 American Society of Civil Engineers.

#### Introduction

Urban expansion results in increasing impervious cover and modifies hydrological processes by reducing runoff response time and increasing peak runoff. In addition, in some regions, increasingly frequent extreme events due to climate change (Kunkel et al. 2020) are overwhelming the stormwater infrastructure capacity causing functional failure before the end of its design life (Mailhot and Duchesne 2010; Swain et al. 2020). Consequently, rainfall-induced urban (or pluvial) flooding has become a common phenomenon in many cities (University of Maryland and Texas A&M University 2018). Replacing and upgrading existing gray stormwater infrastructure (e.g., conduits or detention tanks), is financially and technically challenging due to spatial interdependencies in the coupled infrastructure systems, i.e., interdependencies between drainage conveyance, transportation, and other infrastructure systems (Chester and Allenby 2019; Gilrein et al. 2019). These spatial interdependencies results in lock-in, as past decisions prevent or challenge adaptation of the system. Networked infrastructure, particularly transmission, distribution, or conveyance systems are less

adaptable because they cannot be changed or restructured easily. Furthermore, upgrading the capacity of underground drainage conduits to mitigate localized flooding requires the replacement of several sections of conduits both upstream and downstream. Eventual renewal and replacement of such infrastructure nearing the end of its design life is one of the present-day key issues facing stormwater management (Dolowitz et al. 2018). The inflexible properties of gray stormwater infrastructure motivate the need for alternate design choices, which are adaptable (Manocha and Babovic 2017), flexible, and sustainable. Green stormwater infrastructure (GSI) fills this need while also providing a wide range of co-benefits (Bell et al. 2019; Benedict and McMahon 2002; Choi et al. 2021; Gaffin et al. 2012; Nieuwenhuijsen 2020; Webber et al. 2020). However, the key questions that remain are how the GSI can be distributed across the catchment to achieve the optimum hydrological benefit at least cost, what design criteria shall be considered, and how robust design decisions are in a dynamic environment.

Unlike gray infrastructure, GSI adds flexibility through modularity since it is customizable into numerous design forms, integrable with the existing drainage network, and scalable as the need arises. Different design forms of GSI practices such as bioretention, bioswales, and green roofs, most commonly known as low impact development (LID), are a subset of GSI, engineered to function as a standalone unit or in concert with existing gray infrastructure to enhance hydrological functions of infiltration, storage, and pollutant removal via sedimentation and filtration. Typically, GSI are categorized into systems that are installed on the ground surface (e.g., bioretention and bioswale) and others that are installed above the ground surface (e.g., green roofs). Bioretention is an engineered small depressional area with soil filter media consisting of surface layer, soil layer, and storage layer over native soil, planted

<sup>&</sup>lt;sup>1</sup>Ph.D. Graduate, School of Sustainable Engineering and the Built Environment, Arizona State Univ., Tempe, AZ 85281 (corresponding author). ORCID: https://orcid.org/0000-0002-0106-0318. Email: ashres15@asu.edu

<sup>&</sup>lt;sup>2</sup>Assistant Professor, School of Sustainable Engineering and the Built Environment, Arizona State Univ., Tempe, AZ 85281. ORCID: https://orcid.org/0000-0002-2864-2377. Email: M.Garcia@asu.edu

Note. This manuscript was submitted on April 29, 2022; approved on October 12, 2022; published online on January 11, 2023. Discussion period open until June 11, 2023; separate discussions must be submitted for individual papers. This paper is part of the *Journal of Sustainable Water in the Built Environment*, © ASCE, ISSN 2379-6111.

with native vegetation to promote infiltration and reduce peak runoff (Golden and Hoghooghi 2018). A bioswale is a vegetated channel with trapezoidal cross section or side slopes to collect and infiltrate runoff. Green roofs have a surface layer, a soil layer, and a thin multilayer fabric drainage mat that have limited storage, which is the key difference from bioretention (Rossman and Huber 2016). The shallow soil media in green roofs with native vegetation retain the rainwater and the drainage layer conveys percolated rainwater to a roof drainage system (Mentens et al. 2006). Green roofs are distinguished into two types: extensive, which have thin soil media (≤10 cm); and intensive, which have thicker growing media, allowing for perennial herbs and shrubs, and can be considered as roof gardens (Gregoire and Clausen 2011; Mentens et al. 2006). In both these systems, the hydrologic-hydraulic processes are computed using flow continuity equations that describe change in water content in different layers over time; the details about theoretical background and equations can be found in Rossman and Huber (2016). Bioretention treats direct rainfall and surface runoff it receives from impervious and pervious surface within subcatchments, but green roofs treat only the direct rainfall they receives. Bioretention also involves exfiltration of stored water to native soil as well as an underdrain to a drainage system, whereas a green roof only conveys retained and stored water to a drainage system. By utilizing the impervious roof surface, green roofs provide retention and a limited storage function, which dampen the peak runoff. Such effects could be significant if green roofs are implemented on a catchment scale. Green stormwater infrastructure implemented in several US cities (e.g., Philadelphia, Boston, Seattle) provides evidence that GSI performance meets or exceeds design expectations (Hopkins et al. 2018; USEPA 2014; WEF 2018). Despite growing evidence supporting success stories and performance efficiency, its adoption at the catchment scale remains limited due to uncertainties affecting design and planning (Montalto et al. 2011; O'Donnell et al. 2017; Thorne et al. 2018; Zuniga-Teran et al. 2020). The flexible and modular property of GSI allows it to be integrated as gray-green stormwater infrastructure for capacity enhancement of stormwater system. Such integration requires tools to assess designs and plans at the catchment scale. Further integration of GSI is also subject to availability of space and resources. In the dynamic urban environment with changing urban forms and competing land uses, the delayed action could mean costly GSI implementation or limited design and configuration options, adding further constraint into the planning process.

Urban drainage design standards typically define design precipitation according to the site-specific precipitation intensity, duration, and frequency relationships; produced by federal government agencies, some examples include the National Oceanic and Atmospheric Administration (NOAA) Atlas 14 released in 2004 or older documents, the US Weather Bureau Technical Paper 40 (TP40) released in 1961, and HYDRO 35 released in 1977 (Chow et al. 1998; Lopez-Cantu and Samaras 2018). Historically TP40, which included precipitation estimates for durations from 30 min to 24 h and return periods from 1 to 100 years, was adopted for infrastructure design, but was partially superseded by HYDRO 35 for its events ranging from 5 to 60 min, which was more suitable for urban drainage design (Chow et al. 1998). Currently NOAA's Atlas 14 is the most comprehensive set of precipitation estimates which superseded TP40 and HYDRO 35 across most of the US. Atlas 14 quantifies the 90% confidence interval (CI) for precipitation intensity estimates for durations from 5 min to 60 days and return period of 1 to 1,000 years. These confidence intervals were derived separately for each duration and represent the uncertainties arising from the distribution parameters and record lengths (Perica et al. 2018). Lopez-Cantu and Samaras (2018) studied the variation in precipitation depth estimates between older (i.e., TP40) and newer (i.e., Atlas 14) standardized precipitation analysis documents, and showed that infrastructure failure probabilities changed from 1961 to newer Atlas 14 standard released in 2004. The same study also identified regions and states across the US that need to prioritize changing design standards. Markus et al. (2007) studied variation in 100-year 24-h precipitation estimates from station data, TP-40, Bulletin 70, and Atlas 14 for northeastern Illinois and estimated modeled runoff peaks using HEC-HMS using different estimates, which suggested older design standards could underestimate precipitation depth. The effects of using different standardized precipitation sources or considering uncertainty within an estimate (e.g., Atlas 14 confidence interval), on the design of stormwater infrastructure such as GSI has not been previously studied. Understanding the influence of precipitation uncertainty in stormwater systems also helps to understand the challenges in adaptation planning under the increasing uncertainty due to climate change. As evidence suggests wet extremes have increased in 21st century compared to 20th century across several geographic regions (Stevenson et al. 2022). However, the greater challenge is that the time scale or magnitude of such effects vary geographically (Carvalho 2020; Kunkel et al. 2020).

The dynamics of urban land use due to continuous land development further alters the dynamics of urban flooding, degrades the performance and function of stormwater infrastructure, and constrains the adaptation options to manage flooding. The developed land within and around cities has expanded significantly over the last century across the US. This horizontal growth is typified by two locations and patterns of urban surface change: the city core where urban imperviousness has already reached almost 100% in the last few decades (densification), and surrounding city areas that are expanding outward (sprawl) (Barrington-Leigh and Millard-Ball 2015; USGS 2003). In order to keep the stormwater infrastructure functional the existing infrastructure needs to be adapted to capture increased surface runoff and minimize pluvial flood risk (Arnbjerg-Nielsen et al. 2013). As identifying the optimal configuration of GSI is an integral part of catchment scale GSI planning, understanding how it varies under probable dynamics of such changes helps in GSI decision-making and planning.

The optimal configuration of GSI is defined as the ideal selection of GSI types, amount and spatial distribution over the catchment. For this study we used a fixed standard design specification and parameters for bioretention and green roof as suggested by Rossman and Huber (2016). In this study, we aim to investigate the overarching research question of how the catchment scale optimal configuration of GSI is influenced by uncertainty in design standards and changes in design conditions. Specifically, we first break down this problem into three subquestions:

- How does the uncertainty in precipitation (measured by the confidence interval in Atlas 14) affect the optimal GSI configuration?
- How the change in urban imperviousness affect the optimal GSI configuration?
- Does the uncertainty in precipitation or change in urban imperviousness impose greater influence in GSI configuration in two Phoenix (Arizona) watersheds?

To answer these questions, we use the USEPA's stormwater management model (SWMM) to build a physically based, semidistributed one-dimensional hydrologic-hydraulic model for two urban catchments in Phoenix. These two catchments represent two distinct urban forms, where the urban blocks are already heavily urbanized consisting of commercial buildings (i.e., the urban core) and other has developed over the past 20 years and consists of residential buildings (i.e., sprawl).

**Table 1.** Change in imperviousness from 2001 to 2019, and 90% confidence interval for NOAA Atlas 14 precipitation estimates in 20 most populated US cities

	Δ.	Latitude, longitude for Atlas 14 stations	Atlas 14, 90% CI for 5-year return period, 60-min storm
Location	$\Delta_I$ (%)	(degrees)	(cm)
Austin, Texas	7.56	30.2676, -97.7430	4.72-8.10
San Antonio	7.22	29.4246, -98.4946	4.55–7.80
Phoenix	5.78	33.4483, -112.0758	2.16–3.15
San Jose, California	5.77	37.3387, -121.8854	1.07-1.49
Charlotte, North Carolina	5.77	35.2229, -80.8380	4.65-5.46
Fort Worth, Texas	4.89	32.7510, -97.3309	3.94-6.78
Columbus, Ohio	4.38	39.9620, -83.0027	3.71-4.55
Houston	4.21	29.7608, -95.3695	5.23-8.99
Denver	4.12	39.7400, -104.9920	2.07 - 3.33
Dallas	3.42	32.7782, -96.7951	4.19-7.24
Jacksonville, Florida	3.06	30.3315, -81.6562	5.41-7.75
Indianapolis	2.98	39.7669, -86.1501	3.99-4.90
San Diego	2.09	32.7157, -117.1617	1.57 - 2.27
Washington, DC	1.71	38.8904, -77.0320	4.19-5.11
Philadelphia	1.22	39.9522, -75.1622	4.09-4.85
Chicago	1.18	41.8843, -87.6324	3.96-5.03
New York	1.16	40.7146, -74.0071	3.18-5.11
San Francisco	0.92	37.7771, -122.4196	1.60-2.05
Los Angeles	0.81	34.0536, -118.2454	1.74-2.53
Seattle	0.51	47.6036, -122.3294	N/A

Source: Data from US Census Bureau (n.d.)

### Methodology

#### Catchments Selection

Urban expansion and densification changes imperviousness over time. This process is compared in the 20 largest US cities by population (US Census Bureau, n.d.) (Table 1), using urban imperviousness data from National Land Cover Database, Multiresolution Land Characteristics Consortium available at a spatial resolution of 30 m. The sum of the percent changes in urban imperviousness between 2001 and 2019 was normalized by the total area within the city boundary [Eq. (1)]. The change in urban imperviousness  $(\Delta_I)$  is defined as

$$\Delta_{I} = \frac{\sum_{i=1}^{n} \sum_{j=1}^{m} (I_{i,j}^{2019} - I_{i,j}^{2001}) \times A_{p}}{A_{c}}$$
 (1)

where I = percent imperviousness (for 2001 or 2019); and n and m = rows and columns of the raster data;  $A_p$  = area of a pixel; and  $A_c$  = area of the city. The  $A_c$  is defined as the product of  $A_p$  and number of raster pixels within city boundary ( $N_c$ ). Several of the 20 largest cities are expanding with new impervious surface being added. In general, higher values of  $\Delta_I$  implies greater sprawl and low values implies minimal sprawl over the study period, 2001–2019 (Table 1). The city of Phoenix, which is one of the largest metropolitan regions in the US [Fig. 1(a)] with a population over 1.6 million, represents cities experiencing sprawl where impervious area in city core peaked prior to 2001 and the peripheral area of the city has continued increasing impervious cover [Fig. 1(b)]. Fig. 1(b) shows the change in urban imperviousness in Phoenix at 30 m resolution between 2001 and 2019.

The current uncertainty in the Atlas 14 estimates, as presented through 90% confidence interval (Bonnin et al. 2006), informs

infrastructure designers and decision makers about the potential for over and under design (Table 1). Continued population growth and city expansion increases the demand for new stormwater infrastructure or upgrades of existing infrastructure. In Phoenix, stormwater drainage for streets including catch basin spacing and conduits is required to convey the 2-year return period rainfall (City of Phoenix 2013). However, flooding impacts prompt rethinking of this standard. Extending capacity of infrastructure at frequently flooded locations to handle the 5-year return period rainfall would mitigate flood impacts and increase infrastructure service level and resilience. But once the drainage system is built, replacing its conduits is not a viable solution in many cases, therefore GSI was implemented as the adaptable stormwater management in addition to existing gray infrastructure. For this study we consider 5-year return period rainfall as it is a common stormwater design standard in many regions, and we also purposely stress the existing system to understand how the GSI maintain their level of service under higher rainfall extremes, which many cities globally are expected to experience due to climate change. This pertinent design challenge makes Phoenix an appropriate choice for this study, and the conclusions drawn from this case have implications for other fastgrowing cities. Furthermore, stormwater infrastructure data was comprehensively available for Phoenix.

Despite the hot desert or arid climate (i.e., BWh Köppen classification) with extreme hot summers, mild short winters, and only 204 mm of average yearly precipitation, several locations within Phoenix experience frequent urban flooding. Fig. 1(b) shows that the city has expanded outward in the last two decades. The first catchment selected (Cat. 1) is situated in the Central City neighborhood in downtown Phoenix (DTP), which had a median imperviousness of 79% in 2001 and 81% in 2019; thus Cat. 1 is a representative of area that were fully urbanized in the previous decades [Fig. 1(b)]. The second catchment (Cat. 2), which is situated south of the Central City in the South Mountain Village Phoenix (SMP), had median imperviousness of 15% in 2001 and 45% in 2019; thus Cat. 2 is a representative of an area of urban expansion and densification [Fig. 1(b)]. The details of the stormwater infrastructure feature for Cat. 1 (DTP) [Fig. 1(c)] and Cat. 2 (SMP) [Fig. 1(d)] are implemented in the SWMM model, which is described in next section. The distribution of change in percent imperviousness per pixel value (of 30 m resolution) in Cat. 1 shows the similar left skewed shape for both 2001 and 2019, indicating relatively no change in urban imperviousness between 2001 and 2019 [Fig. 2(a)] while in Cat. 2 the distribution shape of imperviousness has changed from right skewed to symmetrical from 2001 to 2019 [Fig. 2(b)]. Both the hydrologically independent catchments are similar in size with areas of 1.6 km<sup>2</sup> and face frequent flooding [Figs. 3(a and b)]. The rainfall event in Cat. 1 on September 23, 2019 was of 2-year return period and rainfall event in Cat. 2 on August 12, 2014 was of 5-year return period.

# Hydrologic-Hydraulic Model

USEPA's SWMM 5 is a hydrologic-hydraulic model that computes the rainfall-runoff and routing processes, has a low impact development module, and uses dynamic wave routing to solve the complete one-dimensional Saint-Venant flow equations, which account for channel storage, backwater effects, entrance/exit losses, and pressurized flow in stormwater network (James et al. 2010; Rossman 2006, 2017). The stormwater infrastructure data obtained from Phoenix Public Works Department and Flood Control District of Maricopa County consists of all the features and attributes data for stormwater components. The number of stormwater components like conduits and junctions are higher in Cat. 1 compared

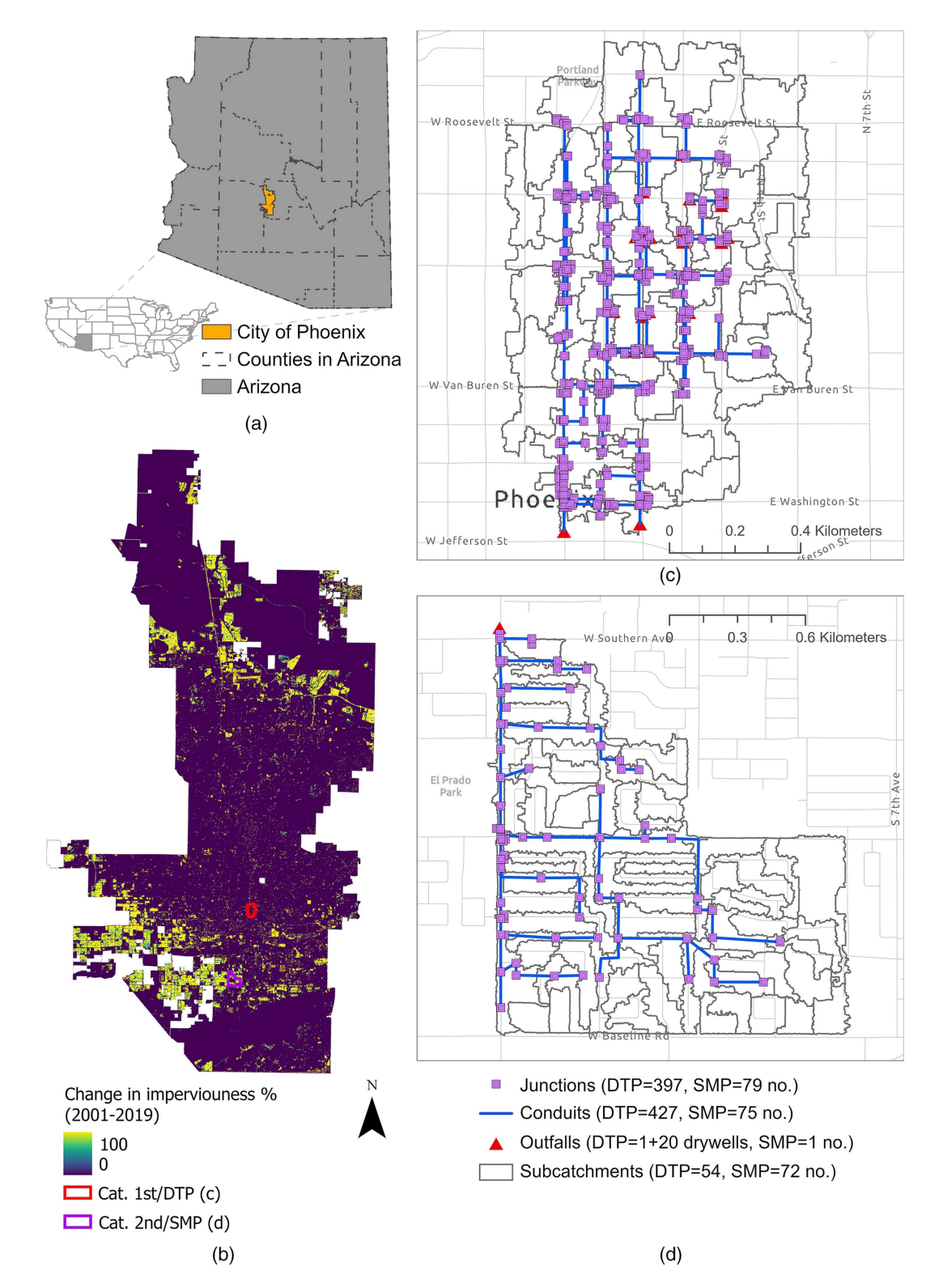


Fig. 1. (a) Location of the city of Phoenix; (b) change in urban imperviousness (%) from 2001 to 2019 and locations of two catchments; stormwater components in (c) Cat. 1, downtown Phoenix (DTP); and in (d) Cat. 2, South Mountain Phoenix (SMP).

to Cat. 2, which has a mix of underground conduits and roadside drains. The 0.3-m resolution LiDAR point cloud data from Arizona State University (ASU) geospatial hub database (ASU 2018) was used to create a digital elevation model (DEM). The DEM was used to extract correct rim and invert elevations for junctions, delineate and discretize subcatchments, and extract width and slope of the subcatchments. The soil types data in two catchments were

obtained from the USDA Natural Resources Conservation Service web soil survey database (USDA-NRCS 2017), and Green-Ampt infiltration parameters (e.g., suction head, saturated hydraulic conductivity) were obtained from the Arizona DOT (ADOT 2014). The soil properties data and urban imperviousness data (MRLC 2021), were extracted into the subcatchment by extracting overlaying polygons and taking average values of pixels contained within each

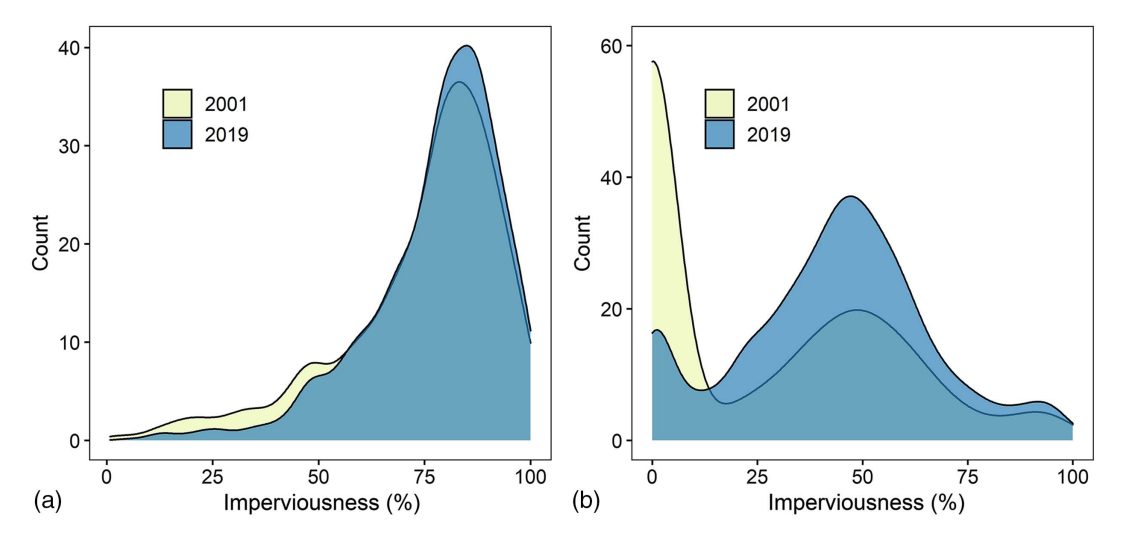


Fig. 2. Change in urban imperviousness (%) from 2001 to 2019 using data from the National Land Cover Database (MRLC 2021) in (a) Cat. 1; and (b) Cat. 2.



**Fig. 3.** Example of flooding (a) in Cat. 1 on September 23, 2019 (reproduced from ASU/NAU 2019, with permission); and (b) in Cat. 2 on August 12, 2014 (reproduced from FCDMC 2014).

subcatchment, respectively, using the ArcGIS's zonal statistics and spatial join tools. We further utilized ArcGIS's hydrology tools and PCSWMM's watershed delineation tools to generate overland flow paths and understand surface flow directions. Based on this information, the runoff generated from both the impervious and pervious portion of each of the discretized subcatchments was routed directly to the closest catch-basin if present, otherwise the runoff from upstream subcatchment is routed to a downstream subcatchment, which eventually drains to the closest catch-basin, and in this case internal runoff routing was also assigned from impervious to pervious surface. For further details on model construction, see Shrestha et al. (2022). The rainfall design storm from Atlas 14 (NOAA and NWS 2021) for 5-year return period, 45-min duration was selected for the GSI configuration experiments. At both the locations the existing gray stormwater system is not able to accommodate runoff from short duration 5-year return period rainfall, and in both the locations GSI offers a flexible way to augment the capacity of the existing conveyance system. The spatial distribution of flooded locations and functional condition of existing infrastructure is measured in terms of (1) the maximum flooding rate at each node which is defined as the peak flooding rate from an overflowing node [note that flooding in the system occurs when hydraulic grade line exceeds rim elevation of the catch basin or manhole for the underground conduits (or street curb height for roadside drains)]; (2) peak runoff from each subcatchment; and (3) duration of exceedance of conduits' capacity, which occurs when a conduit's upstream end is full and hydraulic grade line is greater than conduit slope (James et al. 2010).

## **GSI Optimization**

# **GSI Configuration**

The two types of GSI considered in this study, bioretention and green roofs, were selected as they represent common ground surface and building based GSI types. The availability of space and types of buildings in the two study catchments make these two types of GSIs particularly viable. The size of a single unit of both the bioretention cell and intensive green roof is specified here as 10 m<sup>2</sup>. The design specification and parameters for both types of GSI are shown in the Supplemental Materials (Section S1). The number of GSI units for each variation of bioretention and green roof in Cat. 1, and only bioretention in Cat. 2 is optimized at the subcatchment level. This is because in Cat. 2, the residential houses, do not have suitable flat roofs and thus green roofs are considered not a viable option. The subcatchment layer in SWMM is divided into pervious and impervious segments. The sum of area occupied by streets, buildings and free space constitute the total area of each discretized subcatchments, defined as

Area of subcatchment = Free Space + Roof areas + Streets (2)

© ASCE 04023001-5 J. Sustainable Water Built Environ.

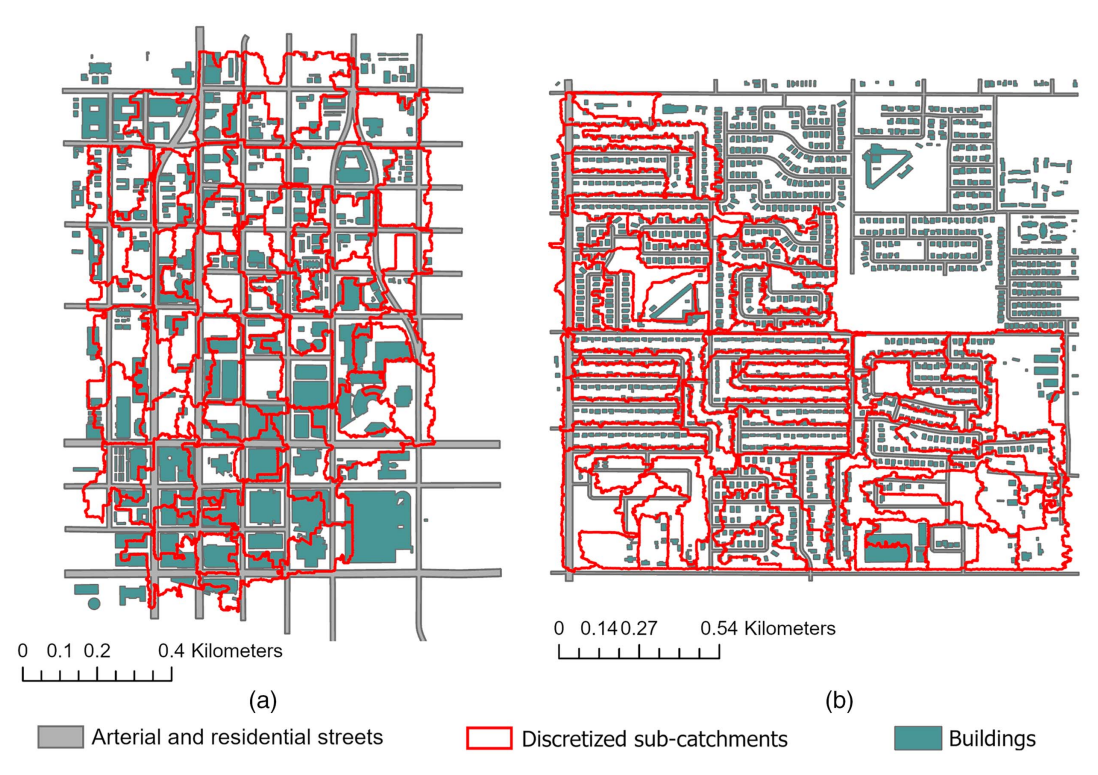


**Fig. 4.** Available space for GSI in each discretized subcatchment is estimated by extracting area occupied by buildings and streets for (a) Cat. 1; and (b) Cat. 2.

Fig. 4 shows the spatial distribution of available space and the built surfaces. The impervious segments are from buildings and streets. In the current GSI implementation, bioretentions are placed only in the pervious segments, and green roofs are placed on buildings. By placing green roofs in the subcatchment, the impervious percent of the subcatchment decreases by the equivalent area occupied by the green roofs as suggested by James et al. (2010). Thus, for each subcatchment in Cat. 1, the corresponding percentage of green roof area relative to its subcatchment area is deducted from the original imperviousness before running each simulation within the optimization algorithm.

#### **Optimization Framework**

The hydrologic-hydraulic models were coupled with a nondominated sorting genetic algorithm that solves multiple optimization problems simultaneously (Blank et al. 2019; Jain and Deb 2014). The nondominated sorting genetic algorithm-II (NSGA-II) is a Pareto-based multiobjective evolutionary algorithm, and a subsequent version of NSGA that uses a Pareto dominance relation for searching entire Pareto front in a single run (Deb et al. 2002; Reed et al. 2013). Several studies have used nondominated sorting genetic algorithm in water resources planning. Kumar et al. (2022) applied NSGA-II to minimize urban runoff volume using optimal size and costs of LIDs. Mwiya et al. (2020) applied NSGA-III for identifying optimal irrigation scheduling to maximize water use efficiency and minimize risk. The implementation of NSGA-II with SWMM 5 model is done in an R environment using R packages swmmr (Leutnant et al. 2019) and nsga2r (Tsou 2013). The size of the population is determined by the number of variables, so the population size for Cat. 1 was 1,080 and for Cat. 2 was 720, and for both the simulations 30 generations were selected. The crossover and mutation probabilities for the NSGA-II algorithm for both the catchments were selected as 0.7 and 0.2, respectively. Each of the optimization simulation experiment was run in 64-bit i7 CPD @ 3.6 GHz processor, which took 60-90 h to complete.

Two objectives were considered in the optimization framework to minimize both the peak flooding (Qpk) resulting from 5-year return period storm and the cost of GSI implementation. The first  $(f_1)$  and second  $(f_2)$  optimization objectives were defined as

$$f_1 = \min\left(\sum_{i=1}^N Qpk_i\right) \tag{3}$$

where Qpk = peak flooding at node i; and N = number of nodes in the model

$$f_2 = \min\left(\sum_{s=1}^{N} \text{Cost}_s\right) \tag{4}$$

where Cost = capital cost for construction of GSIs in subcatchments (it does not reflect life cycle cost); and N = number of subcatchments in the model. The optimization is constrained by the availability of space for GSI implementation, which is defined as  $0 \le AGI_S \le AGI_M$  where  $AGI_S$  is the area of assigned GSI, and  $AGI_M$  is the maximum allowable area for GSI, which is maximum roof area for green roof installation and maximum free space for bioretention installation in each subcatchment.

Each parameter value  $\{p_1, p_2, \ldots, p_n\}$  represents the number of GSI to be implemented in each subcatchment. The minimum and maximum value of these parameters is defined as,  $P_l = \{p_1, p_2, \ldots, p_n\}$  and  $P_u = \{p_1, p_2, \ldots, p_n\}$  where  $P_l$  is the set of lower bounds with  $p_1, p_2, \ldots, p_n = 1$ , and  $P_u$  is the set of upper bounds with  $p_1, p_2, \ldots, p_n$  determined by maximum space available for parameter value for n = 108 (for Cat. 1) and n = 72 (for Cat. 2) corresponding to number of discretized subcatchments and types of GSI implemented. The assignment of a number of GSI units for every subcatchment within the fitness function is defined as

$$NGI_S = \text{round}\left(\min\left(\frac{AGI_M}{GI_U}, p_{an}\right)\right)$$
  
 $\forall S \in \{S_1, \dots, S_N\} \text{ subcatchments}$  (5)

where  $p_l \le p_{an} \le p_u$ ;  $GI_U =$  unit area of GSI; and the min $\{[(AGI_M)/(GI_U)], p_{an}\}$  function ensures that the space constraint is maintained. The total cost of green stormwater infrastructure is defined as

$$Cost = \sum_{S=1}^{N} NGI_S \times GI_U \times cp \quad \forall S \in \{S_1, \dots, S_N\} \quad (6)$$

where cp = standard capital cost per unit square meter of GSI installation, which is \$430/m² for bioretention and \$332/m² for green roof (Rutgers 2017; Terrascope 2022). The graphical results from SWMM model outputs and optimization simulation presented in the following section was developed using ArcGIS Pro tool and ggplot2 package in R (Wickham 2009).

#### Results

For Cat. 1 in Central City, Phoenix the best fit rainfall estimate from Atlas 14 for 5-year (2-year) return period for 1 h duration is 2.59 cm (1.74 cm), while the 90% confidence interval are 2.15 cm (1.46 cm) and 3.15 cm (2.12 cm). For Cat. 2 in South Mountain, Phoenix, for 5-year (2-year) the mean is 2.59 cm (1.77 cm) and 90% confidence interval are 2.16 cm (1.48 cm) and 3.17 cm (2.16 cm). Using 5-year return period design storm both the catchments experience flooding at multiple locations before GSI is adopted [Figs. 5(a-i)]. The first row [Figs. 5(a-c)] shows the model simulation result for Cat. 1 for 2019, which is representative for 2001 as well since the imperviousness remained unchanged. The second and third rows [Figs. 5(d-i)] show the model simulation for Cat. 2 for 2001 and 2019 conditions, respectively. The increasing impervious area as shown in Fig. 2(b) in Cat. 2 generates higher runoff and peak flood in 2019 as compared to 2001. Generally, the higher runoff from subcatchments is generated if the urban imperviousness is higher. But also, if the subcatchment receives runoff from upstream subcatchments, such as top-right subcatchments in Cat. 1 [Figs. 5(a-c)] and bottom right subcatchments in Cat. 2 [Figs. 5(d-i)]. With the

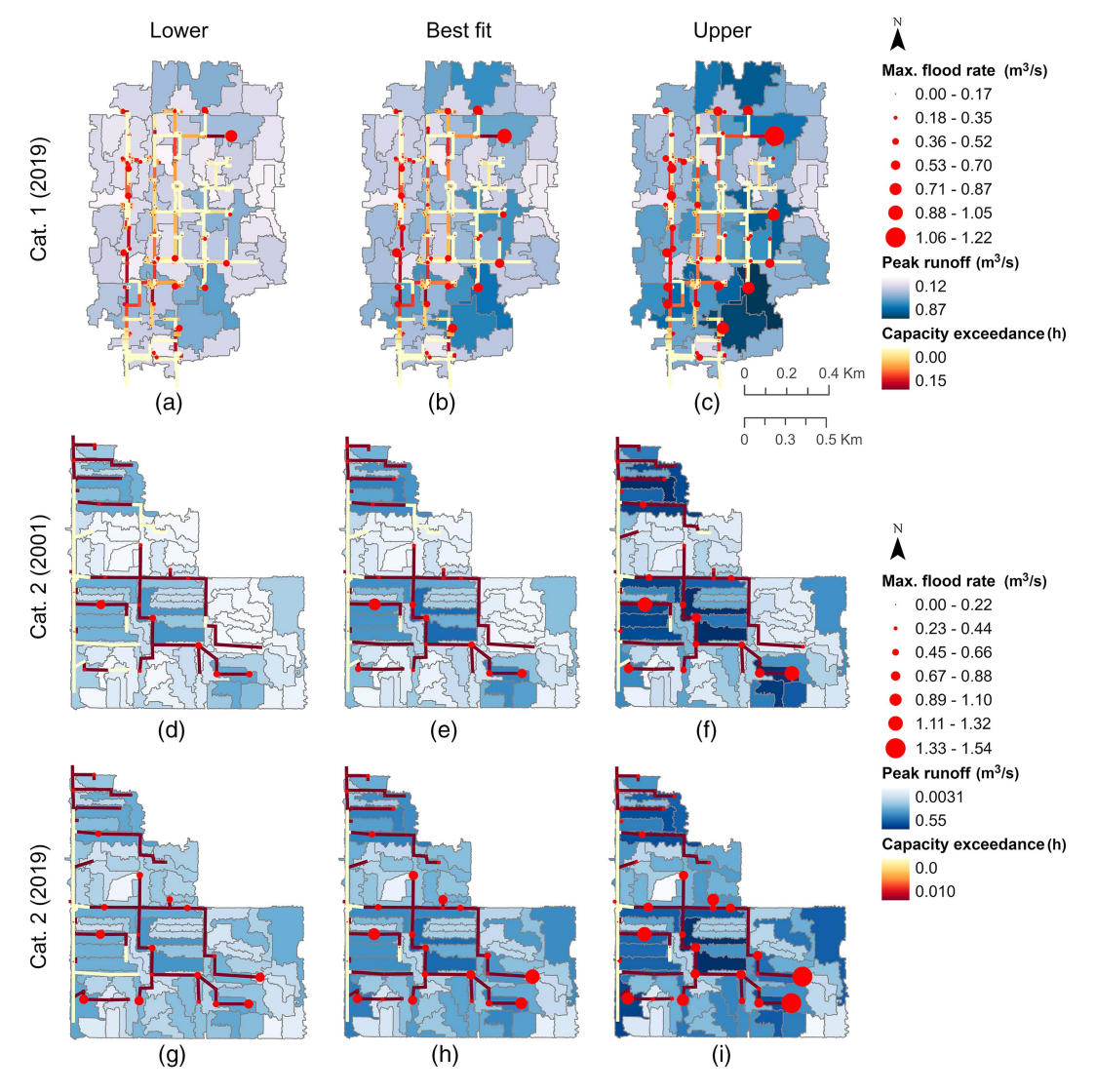


**Fig. 5.** Pre-green infrastructure condition under best fit and confidence intervals (i.e., lower and upper values) of the Atlas 14 5-year return period rainfall estimates as simulated by SWMM showing the maximum flood rate from flooded junctions, peak runoff from subcatchments, and the duration of exceedance of conduits' capacity at the imperviousness level for (a–c) 2019 for Cat. 1; (d–f) 2001 for Cat. 2; and (g–i) 2019 for Cat. 2.

absence of stormwater network and catch basin to transport runoff, instead the flow is routed to the downstream subcatchments, thus the receiving subcatchment generate peak runoff and receiving junctions generate the peak flooding. Note that outfalls for Cat. 1 are in the south of the catchment, and for Cat. 2 it is in the north of the catchment as shown in Figs. 1(c and d).

The maximum flooding rate from nodes and peak runoff from subcatchments increases as the rainfall estimates change from lower, best fit to upper bound of the Atlas 14 confidence intervals for both the catchments across time [Figs. 5(a–i)]. GSI, sited within a subcatchment, reduces the peak runoff from that subcatchment, subsequently reducing pressure on downstream conduits. The optimization algorithm seeks a quantity and spatial distribution of GSI across subcatchments that minimizes the objectives.

# Effects of Uncertainty in Design Precipitation Estimates

Figs. 6(a–i) illustrate the results of the multiobjective optimization and show the Pareto optimal solutions. The black points are the nondominated Pareto optimal solution with the first Pareto front rank and gray points are the remaining dominated solutions. For Cat. 1, there is slight difference between imperviousness of 2001 and 2019, but for Cat. 2 there are significant differences [Figs. 2(a and b)]. Thus, results for Cat. 1 include that of the 2019 conditions [Figs. 6(a–c)] (which also represents 2001 condition) and for Cat. 2, which includes both years [Fig. 6(d–i]. The first column

[Figs. 6(a, d, and g)] shows the results for the lower bound of the confidence interval of the design storm (i.e., lower estimate), the second column [Figs. 6(b, e, and h)] shows the result for best fit value (i.e., best fit estimate) and third column [Figs. 6(c, f, and i)] shows the result for upper bound of the confidence interval (i.e., upper estimate).

For Cat. 1 [Figs. 6(a-c)], the Pareto front shifts upward as we move from lower to upper bound of the Atlas 14 design rainfall estimates, indicating that achieving a given level of flood control comes at a higher cost. The solutions are selected first by selecting solutions that can totally mitigate flooding and second the least cost solution among them as shown by the intersection of solid lines in Figs. 6(a-c). The cost of mitigating flooding using GSI increases by 49%–77% from the lower to best fit and best fit to upper estimates [Figs. 6(a-c)]. Fig. 7 further illustrates this selected solution by showing the number of GSI units required to mitigate flooding resulting from 5-year return period 45-min storm. The number of required bioretentions (with unit area of 10 m<sup>2</sup>) increased from 11,046 to 28,649, which is 0.11 km<sup>2</sup> to 0.28 km<sup>2</sup>, while depending on the design standards from lower to upper bound of the Atlas 14 design rainfall estimates [Figs. 7(a-c)]. Similarly, the number of required green roofs (with unit area of 10 m<sup>2</sup>) increased from 6,257 to 16,696 (in area: 0.06 km<sup>2</sup> to 0.16 km<sup>2</sup>) [Figs. 7(d-f)]. Also note that the algorithm was able to prioritize the subcatchments, which are the likely source of flooding in Cat. 1, by adopting bioretention or green roofs on those areas [Figs. 5(a–c) and 7(a–f)]. Prioritizing these locations reduces the total cost and amount of

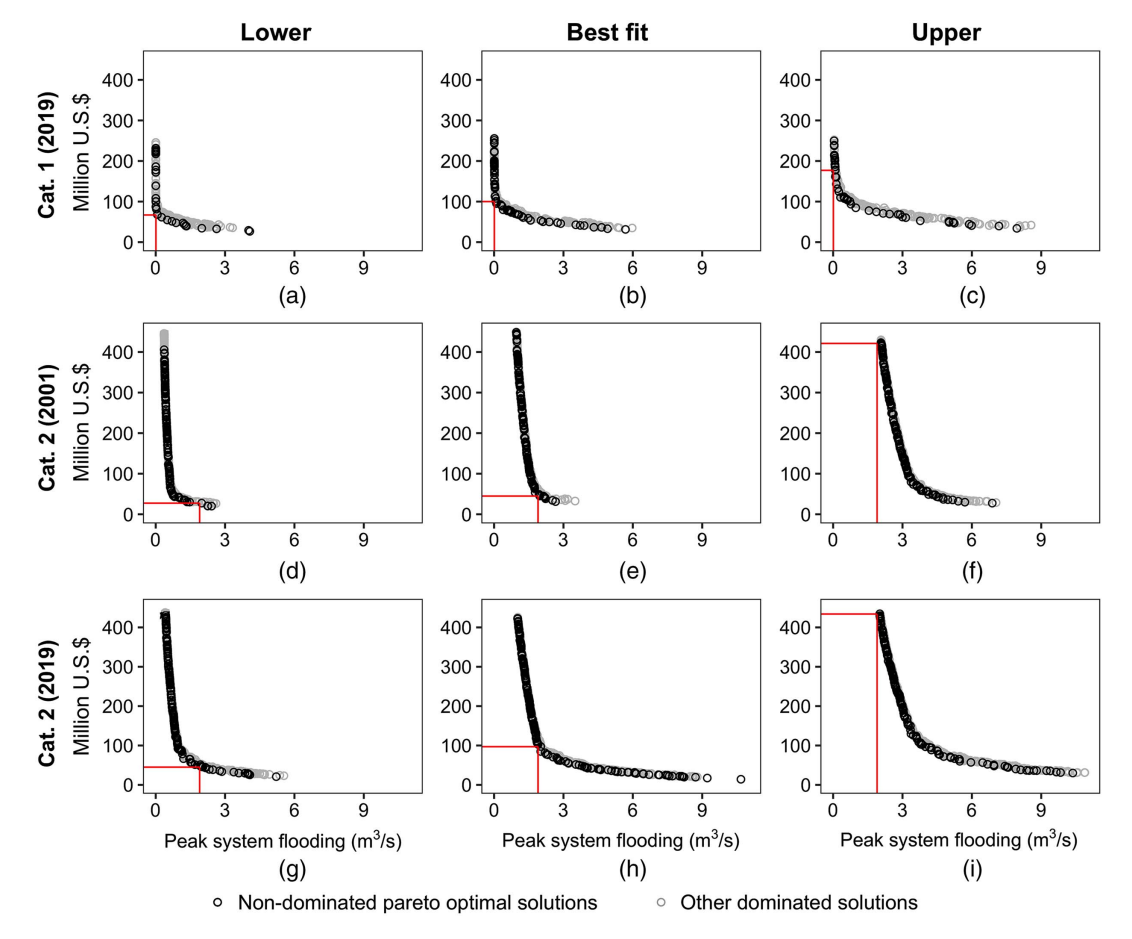


**Fig. 6.** Pareto optimal solution for GSI installations to reduce the peak system flooding using best fit and confidence intervals (i.e., lower and upper values) of the Atlas 14 estimates at the imperviousness level for (a–c) 2019 for Cat. 1; (d–f) 2001 for Cat. 2; and (g–i) 2019 for Cat. 2. Intersection of solid lines are the selected solution for further analysis (see Figs. 7 and 8).

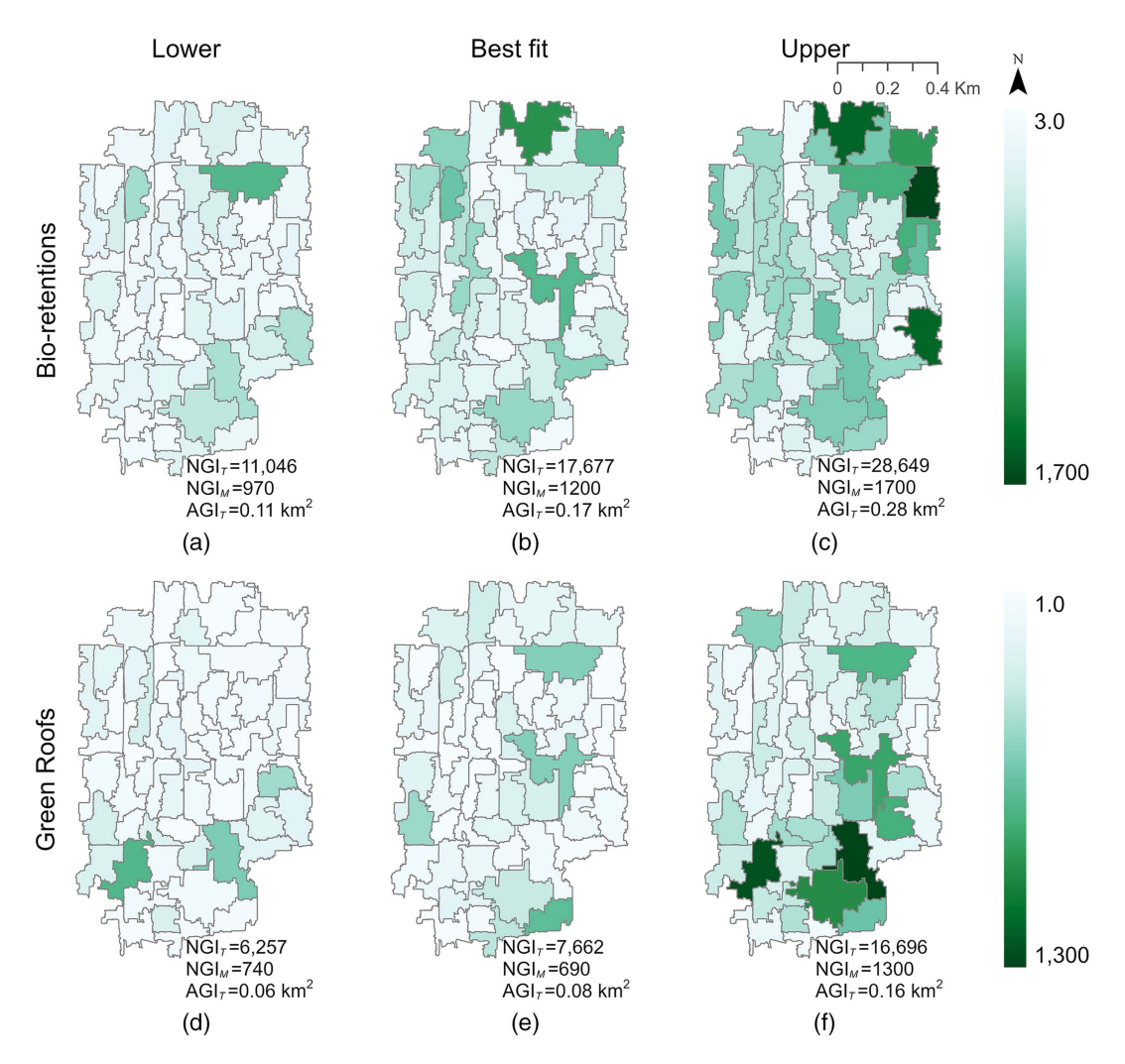


**Fig. 7.** Optimal configuration of GSI (bioretentions and green roofs) at least possible cost in Cat. 1 for mitigating peak flooding. Panels show the (a–c) number of bioretentions; and (d–f) green roofs required.  $NGI_T$ ,  $NGI_M$ , and  $AGI_T$  refer to the total number, maximum number in any of the subcatchments, and total area of GSI required. Scale 1–1,300 or 1,700 is the number of GSI per subcatchment.

GSI required. We also observed some stochasticity wherein GSI are spatially distributed while searching for a solution between maximum flood reduction and minimum cost. As such, the number of GSI in some sub-catchments [e.g., upper right in Fig. 7(a)] decreased while using best fit estimate compared to while using lower estimate but increased again in using upper estimate [Figs. 7(b and c)]. To further understand the effect of the rainfall estimates on the amount of GSI required, we examined how the increase in precipitation depths by 5% to 50% compared to the best fit estimate will influence the GSI configuration, as shown in the Supplemental Materials (Section S2). The flooding conditions under a 5-year return period as shown in Figs. 5(a-i), will only be exacerbated if climate change results in an increasing frequency and magnitude of extreme events. The incremental change of rainfall intensities from 5%-50% shows the increase in residual flooding and the higher investment required to meet flood reduction plans, which reflects the challenges due to climate change (Fig. S1). Such effects presented here only for Cat. 1 will hold true for Cat. 2 and in general most urban catchments.

For Cat. 2, minimizing the peak flood is constrained by the availability of space, as only bioretention was adopted due to the absence of flat roofed buildings. Cat. 2 is a dense residential neighborhood with single to multifamily residential homes with

pitched roofs not feasible for green roofs. This restriction resulted in higher residual flooding when best fit and upper estimates were implemented [Figs. 6(e and f)]. When the lower estimate is used, the flooding is almost eliminated [Fig. 6(d)]. Here we see that within the confidence interval, different precipitation estimates could result in drastically different levels of flood risk and cost of flood mitigation. The Pareto optimal solution showed drastically higher residual flooding for a given GSI investment using lower to upper bound of the Atlas 14 design rainfall estimates [for both 2001 and 2019 conditions; Figs. 6(d-f) and (g-i)]. From the Pareto front for 2001, while using lower Atlas 14 estimate the least GSI investment resulted in flood reduction (residual flooding) to 2.4 m<sup>3</sup>/s [Fig. 6(d)]. Residual flooding is referred to as flooding that GSI could not completely mitigate. However, using best fit and upper estimates for precipitation intensity resulted in flood reduction potential to 2.5 m<sup>3</sup>/s [Fig. 6(e)] and 7 m<sup>3</sup>/s, which is higher residual flooding compared to lower precipitation intensity estimate [Fig. 6(f)]. Since there are residual flooding still existing after higher investment for GSI implementation specially while using best fit and upper estimate, the maximum flood reduction goal the system can meet is reducing peak flooding to 2 m<sup>3</sup>/s. A solution representing this flood reduction goal at least cost investment is selected from all six Pareto fronts [Fig. 6(d-i)], which is further

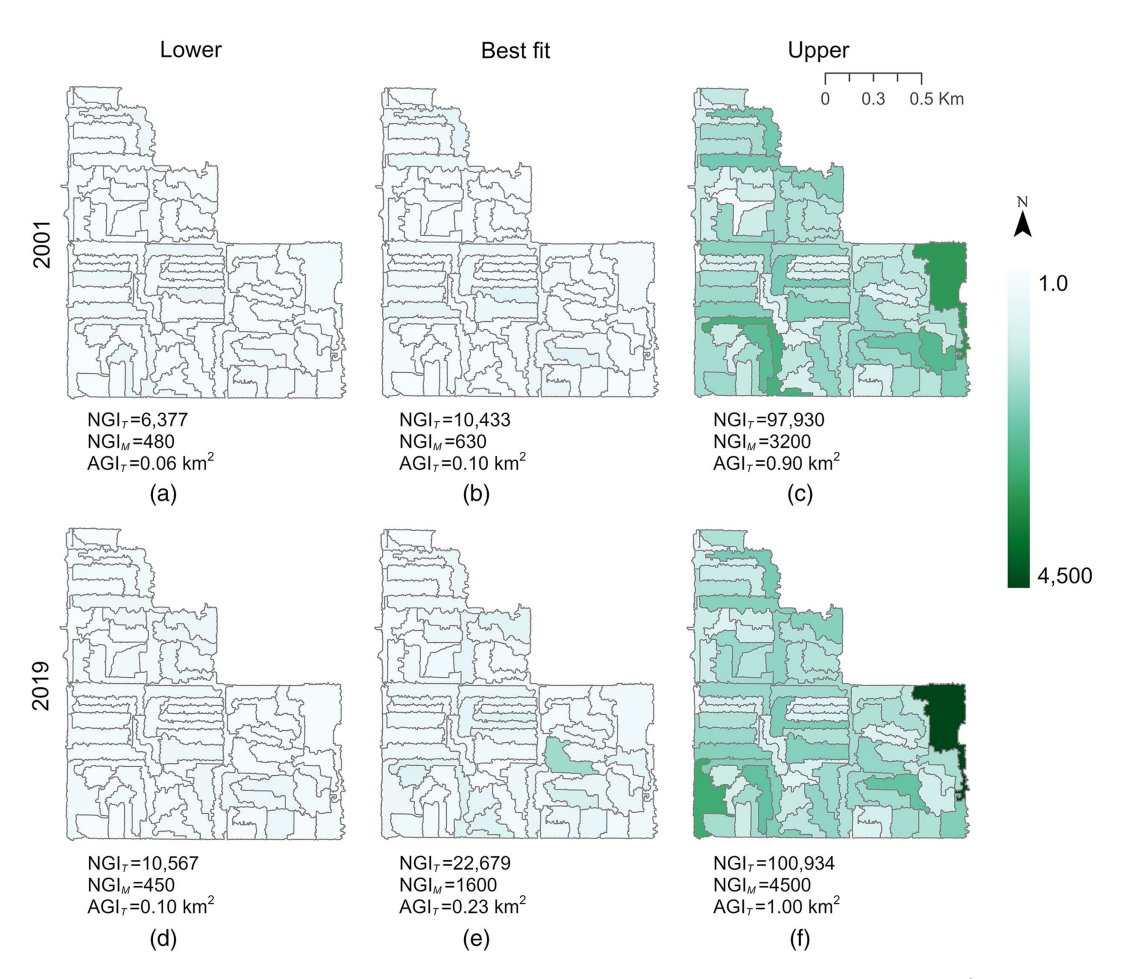


**Fig. 8.** Optimal configuration of GSI (bioretentions) at least possible cost in Cat. 2 for reducing peak flooding to 2 m<sup>3</sup>/s. Panels show the number of GSI required in imperviousness level for (a–c) 2001; and (d–f) 2019. The maximum flood reduction possible is  $Q_{pk} = 2$  m<sup>3</sup>/s given the constraints, and NGI<sub>T</sub>, NGI<sub>M</sub>, and AGI<sub>T</sub> refer to total number, maximum number in any of the subcatchments, and total area of GSI required. Scale 1–4,500 is the number of GSI per subcatchment.

analyzed in Fig. 8. From these selected solutions, the cost of flood reduction using GSI increases while using lower to best fit estimate and best fit to upper estimate by 85%–835% for 2001 conditions [Figs. 6(d-f) and 8(a-c)] and 115%–348% for 2019 conditions [Figs. 6(g-i) and 8(d-f)]. Using the lower, best fit, and upper estimates would require  $6,377,\ 10,433,\$ and 97,930 numbers (in area:  $0.06\$ km²,  $0.1\$ km² and  $0.90\$ km²) of bioretentions in the 2001 condition. In the 2019 condition it would require 50%–100% more.

Similar, to Cat. 1, the optimization algorithm was able to target the subcatchments that have the highest runoff or one which is at the proximity to the capacity constrained conduits and flooded nodes [Figs. 5(d–i) and 8(a–f)]. The optimization algorithm allows bioretention to be placed only in open space. Thus, in absence of available space within the subcatchment where there is higher runoff and peak flooding, the nearby subcatchments are instead chosen for GSI implementation.

Also note that the cost of flood reduction in Cat. 2 is higher than in Cat. 1, primarily due to the lower amount of existing underground gray-infrastructure in Cat. 2 to convey stormwater and because the cost of bioretention is 1.3 times that of green roofs. The implementation of green roofs further reduces the peak runoff by retaining the precipitation and conveying the excess water back into the drainage system slowly, which is an additional advantage in Cat. 1. Most of the extended urban areas since 2001 or earlier around Cat. 2 in Phoenix do not have an extensive network of gray stormwater infrastructure, which presents another challenge in

flood management. The analysis on optimal configuration due to change in imperviousness is presented next.

#### Effects of Changes in Urban Imperviousness

The increase in urban imperviousness results in two different patterns of catchment response in Cat. 2: (1) an increase in the amount of flooding in previously flooded locations, and (2) flooding in new locations as shown by the changes in the maximum flood rate and change in peak runoff in Figs. 5(d-i). The optimal GSI configuration under these conditions as computed for two periods, shows that amount of investment required to mitigate the same amount of flooding in 2019 could be significantly higher than in 2001 [Figs. 6(d-i)]. For example, using the best fit estimate for the design storm, the investment of \$50 million could achieve the maximum flood reduction to 2 m<sup>3</sup>/s [Fig. 6(e)]. However, under the 2019 condition, the residual flooding increased as the same investment could only achieve peak flood reduction to 4 m<sup>3</sup>/s [Fig. 6(h)]. Fig. 8 shows the number of GSI installations (assuming a 10 m<sup>2</sup> area) required to reduce the flooding resulting from 5-year return period 45-min storm to 2 m<sup>3</sup>/s, based on a selected solution for this analysis as discussed previously, which is also shown in Figs. 6(d-i). Note that under the given space constraint the full mitigation of flooding is not possible here and results in residual flooding. The number of GSI installations required to achieve the same level of flood reduction increases from 6,377 to 10,567

(using the lower estimate), 10,433 to 22,679 (using the best fit estimate), and 97,930 to 100,934 (using the upper estimate) from the 2001 to the 2019 land use (Fig. 8). As the system receives more intense rainfall by moving from the lower to upper bound of rainfall estimates, the allowable capacity for GSI reaches its limit and reducing flooding becomes more difficult even with higher GSI investment. The effect of uncertainty from the confidence interval in 5-year return period rainfall estimate in optimal GSI requirement is much larger compared to the effect of land use change that happened between 2001 and 2019.

#### **Discussion**

# GSI Design for Pluvial Flood Management

The optimal catchment scale benefits from GSI are sought by identifying GSI configurations with optimal amount, type, and spatial distribution within the catchment. The multiobjective optimization algorithm in combination with a physically based hydrologichydraulic model (e.g., SWMM) is useful in identifying global optimal solutions while evaluating the tradeoff between objectives. Pareto fronts showing tradeoffs between objective of flood mitigation or reduction and investment required showed the diminishing return for same amount of GSI investment [Figs. 6(a-i)]. This is because in search of optimal placement of GSI, the most effective discretized subcatchments that return maximum flood reduction are filled with GSI first followed by less effective subcatchments. Consistent with recent work in arid catchments (Li and Burian 2022), the results show that both increasing precipitation intensity and land change can worsen pluvial flooding. However, here we find that variation in design storm precipitation within the confidence interval for the 5-year, 45-min Atlas 14 storm has a greater impact than land use in a Phoenix catchment that experienced a median 30% increase in imperviousness. Note that Cat. 2 is located in one of the neighborhoods with the highest 2001-2019 increase in imperviousness (Fig. 1) and that Phoenix is one of the large cities with the greatest increase in imperviousness in the US over the same period (Table 1).

The approach presented in this paper can be extended to larger catchments or to different spatial discretization such as the parcel or block. The objective used here is to minimize overall flooding in the system while controlling cost. Alternate objectives of enhancing infiltration or storage, removing runoff pollutants, prioritizing critical locations or other planning goals might warrant different configurations or new designs. By simultaneously optimizing bioretention and green roofs across the constraint of space and searching for cost-effective solutions, the algorithm determined the optimum or Pareto optimal solutions with exact number of bioretention and/or green roofs. This method can be adapted to prioritize one over the other by adding additional constraints, e.g., assigning priorities for land use to limit expansion of bioretention. It should further be noted that with current objective, the algorithm is able to prioritize the GSI where it is required the most, i.e., subcatchments where there is higher runoff and flooding. The assumption in this study is that land is feasibly available based on free space, and we have not considered land value or land use priorities, but this approach and tool can be adapted to accommodate different constraints and priorities relevant to planning process. For example, the optimization framework can be modified to prioritize areas where consequences of flooding are high such as medical or school zones or densely populated areas. The multiobjective framework can also be a useful planning tool to study the tradeoff across prioritizing particular area for flood protection, resources, and cost of implementation and maintenance. The long-term performance variation of GSI, life-cycle cost, benefit-cost ratio, and net present value are some of the on-going research efforts in implementing GSI; future research should focus of the cost of delayed decision of implementing GSI (Bernagros et al. 2021; DelGrosso et al. 2019) if a flexible planning approach is to be adopted (Eckart et al. 2012).

### GSI Adaptation under Uncertainty

The current uncertainty in Atlas 14 estimates could result in a risk of over or under building stormwater capacity. If the best fit estimate is chosen it could result in over building the system if the true 5-year event is indeed closer to the lower bound of the confidence interval and vice versa. In terms of GSI, this could result in 8,036 numbers of GSI installations (or 0.08 km² of GSI with unit area of 10 m²) being unnecessary if it is over built or facing functional failure if under built as shown for Cat. 1 in Fig. 7. The risk of over and under building is comparatively higher for Cat. 2 as there is currently inadequate gray infrastructure [Figs. 1(b) and 8]. This risk is amplified when there is uncertain land use change [Figs. 8(d–f)].

However, the flexibility and modularity of GSI reduces the risk of over or under design (Gilrein et al. 2019). Following the principles of flexible design, after initial GSI is installed, additional modules may be added over time as warranted by changes in land use or by either changes in or misestimation of the design storm (De Neufville and Scholtes 2011). As such these uncertainties are not barriers to GSI adoption but an opportunity to identify the risk in design and construction and implement appropriate adaptation strategies under uncertainty. Further, learning over time will reduce uncertainties with respect to design storm estimates and the impacts of climate change. For example, applying Bayesian learning to climate uncertainty over time can be used to inform planning strategies (Fletcher et al. 2019). A similar framework could be used to inform implementation of GSI over time as part of a flexible planning approach.

The results (Figs. 6–9) also illustrate that GSI is not a panacea, particularly if high precipitation estimates are accurate or if short duration precipitation intensifies with climate change. The GSI required to mitigate flooding for the high estimate of precipitation covers 0.44 km² or 27.5% of Cat. 1, and 0.9 km² or 56.3% of Cat. 2 with 2001 land use and 1.0 km² or 62.5% of Cat. 2 with 2019 land use. While technically feasible given the definition of free space used in the optimization routine (all land that is not street or building), this level of GSI implementation is unrealistic from a

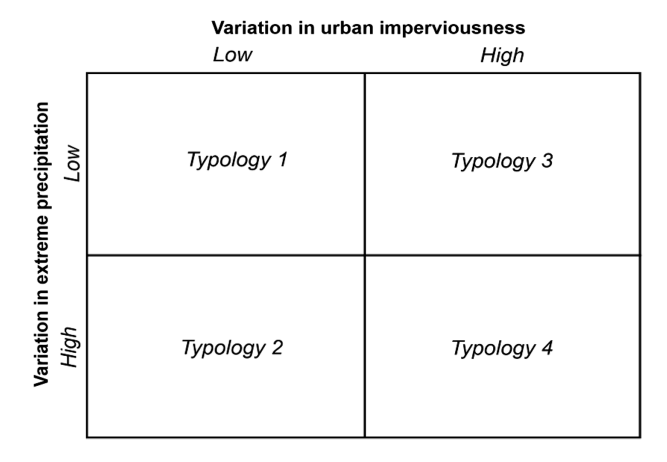


**Fig. 9.** Dynamics of change occurring across cities that will potentially influence GSI planning.

practical standpoint due to other competing land uses. GSI can be part of the solution; however, when the drainage system is significantly underbuilt, GSI alone will often be insufficient. As presented in Figs. 6(d–i), the high cost of GSI implementation in Cat. 2 means GSI is not a replacement for sufficient gray-infrastructure. Instead, the integration of gray-green stormwater infrastructure is needed, where GSI can incrementally add capacity as needed.

#### Reflections on Other US Cities

The confidence interval for Atlas 14 precipitation estimates, particularly for shorter storm durations relevant for stormwater infrastructure design, varies across cities. Similarly, the change in imperviousness varies across and within cities. Understanding the historic city expansion and future probable direction for urban expansion, and uncertainty in design rainfall estimates helps the decision-makers to understand risk of over- or underbuilding stormwater capacity. Furthermore, future uncertainty due to climate change not incorporated in Atlas 14 estimates, will layer on the uncertainty in current design rainfall estimates, further complicating the GSI planning process and such changes will not be uniform across cities. We can conceptualize these dynamics created by the combination of climate change and land use change into four typologies (Fig. 9). The risk of drainage system functional failure is low in Typology 1 and highest in Typology 4. The two catchments presented in this study for Phoenix represent low and high change in urban imperviousness. Most of the other cities with higher  $\Delta_I$ that are continuously expanding outward experience both the low (in the city core) and high (at satellite cities or suburbs) change in imperviousness. Comparison between the variation in imperviousness (i.e., Typologies 1 versus 3, or Typologies 2 versus 4) in the areas that experience a high increase in imperviousness (Typology 3 or 4) present a more complex challenge of optimal GSI planning. This is particularly true for catchments that have highly permeable soils, which result in greater loss of infiltration function. The majority of soils in Cat. 2 are Estrella loam and Antho sandy loam with moderate hydraulic conductivity in of 0.07-0.3 cm/h (ADOT 2014; USDA-NRCS 2017). This study also showed that higher variation in the design storm precipitation, which could be exacerbated by climate change, combined with relatively lower change in imperviousness (i.e., Typology 2) can have greater uncertainty compared to the catchment that experiences a higher change in imperviousness but a lower change in precipitation (i.e., Typology 3).

A limitation of this study is the focus on a single city, Phoenix, with flat topography, a gridded stormwater conveyance system, and deep groundwater. In catchments with different topography or network design, or with shallow groundwater, the responses to precipitation and land use change may vary. This study is also limited by the range of soil types found in these study catchments. As discussed previously, the rainfall-runoff response is more sensitive when soils with high infiltration rates are replaced by impervious surfaces. Lastly, the standard GSI specification used in practice was used for this study. However, this should be compared against performance of GSI practices in the field. Although these limitations suggest case specific analysis for GSI planning, understanding where the catchment and cities are within the four typologies helps planners and designers to assess risk based on two key characteristics.

#### **Conclusions**

This study investigated the impacts of precipitation uncertainty and land use change on the optimal configuration of GSI by applying a coupled hydrologic-hydraulic model (SWMM) and an optimization

algorithm (NSGA-II) in two study catchments in Phoenix. The GSI configuration defined for this study as the type, amount and spatial distribution of GSI, where considered types include bioretention and green roofs. Based on the results of this analysis, we present the following conclusions:

- While both increasing precipitation intensity and land change can worsen pluvial flooding, variation in precipitation estimates within the confidence interval for the 5-year, 45-min storm Atlas 14 storm has a greater impact than land use in a Phoenix catchment that experienced a median 30% increase in imperviousness. This effect is sensitive to soil type, with catchments with higher soil hydraulic conductivity expected to display a stronger response to land use change. However, the results highlight the importance of considering precipitation uncertainty in stormwater design.
- The uncertainty in design storm precipitation and the potential degree of near-term land use change (~20 years) collectively result in a wide range of optimal GSI configurations. If designing a traditional gray-infrastructure system (i.e., stormwater conduits) this would present a significant risk of over or underbuilding. This risk highlights the benefit of the modular nature of GSI, which can be incrementally deployed over time as land use conditions change or the best estimate of design storm precipitation is updated.
- The results also show that GSI is not a panacea and cannot mitigate all flooding impacts even within the Atlas 14 design storm confidence interval. This indicates that relying on GSI to adapt to climate change–driven increases in precipitation intensity may be beneficial but inadequate on their own.

Limitations of this study point to the need for future research efforts. While this study placed the case of two Phoenix catchments in the context of land use trends and precipitation uncertainty in large US cities broadly, further research should investigate the impact of local catchments characteristics on the effects found in this paper.

## **Data Availability Statement**

All the data except stormwater infrastructure data and all the codes that support the findings of this study are available from the corresponding author upon reasonable request. Some data used to build the model is available as indicated in the text. Direct requests for other data may be made to the provider as indicated in the Acknowledgements.

#### Acknowledgments

This work is supported by National Science Foundation (NSF) Smart and Connected Communities Program (1831475). The data for analysis and model building had been provided by Phoenix Public Works and Flood Control District of Maricopa County.

#### **Supplemental Materials**

Table S1 and Fig. S1 are available online in the ASCE Library (www.ascelibrary.org).

### References

ADOT (Arizona DOT). 2014. Highway drainage design manual volume 2— Hydrology. Phoenix: ADOT.

© ASCE 04023001-12 J. Sustainable Water Built Environ.

- Arnbjerg-Nielsen, K., P. Willems, J. Olsson, S. Beecham, A. Pathirana, I. Bülow Gregersen, H. Madsen, and V. T. V. Nguyen. 2013. "Impacts of climate change on rainfall extremes and urban drainage systems: A review." Water Sci. Technol. 68 (1): 16–28. https://doi.org/10.2166/wst.2013.251.
- ASU (Arizona State University). 2018. "Metro Phoenix USGS LiDAR data." Accessed November 1, 2020. https://asu.maps.arcgis.com/apps/webappviewer/index.html?id=0372792855514dd3bf9654c20bbe 10e6.
- ASU/NAU (Arizona State University/Northern Arizona University). 2019. "FloodAware." Accessed March 1, 2020. https://floodaware.net/.
- Barrington-Leigh, C., and A. Millard-Ball. 2015. "A century of sprawl in the United States." *Proc. Natl. Acad. Sci. U.S.A.* 112 (27): 8244–8249. https://doi.org/10.1073/pnas.1504033112.
- Bell, C. D., K. Spahr, E. Grubert, J. Stokes-Draut, E. Gallo, J. E. McCray, and T. S. Hogue. 2019. "Decision making on the gray-green stormwater infrastructure continuum." *J. Sustainable Water Built Environ.* 5 (1): 04018016. https://doi.org/10.1061/JSWBAY.0000871.
- Benedict, M. A., and E. T. McMahon. 2002. "Smart conservation for the 21st century." Green Infrastruct. 20 (Jun): 12–17.
- Bernagros, J. T., D. Pankani, S. D. Struck, and M. E. Deerhake. 2021. "Estimating regionalized planning costs of green infrastructure and low-impact development stormwater management practices: Updates to the US Environmental Protection Agency's national stormwater calculator." J. Sustainable Water Built Environ. 7 (2): 04020021. https://doi.org/10.1061/JSWBAY.0000934.
- Blank, J., K. Deb, and P. C. Ro. 2019. "Investigating the normalization procedure of NSGA-III." In *Evolutionary multi-criterion optimization*, edited by K. Deb, E. Goodman, C. A. Coello Coello, K. Klamroth, K. Miettinen, S. Mostaghim, and P. Reed, 229–240. Cham, Switzerland: Springer International Publishing.
- Bonnin, G. M., D. Martin, B. Lin, M. Yekta, and D. Riley. 2006. *Precipitation-frequency atlas of the United States volume i version 4.0: Semiarid southwest (Arizona, Southeast California, Nevada, New Mexico, Utah)*. Silver Spring, MD: National Weather Service.
- Carvalho, L. M. V. 2020. "Assessing precipitation trends in the Americas with historical data: A review." Wiley Interdiscip. Rev. Clim. Change 11 (2): 1–21. https://doi.org/10.1002/wcc.627.
- Chester, M. V., and B. Allenby. 2019. "Toward adaptive infrastructure: Flexibility and agility in a non-stationarity age." Sustainable Resilient Infrastruct. 4 (4): 173–191. https://doi.org/10.1080/23789689.2017 1416846
- Choi, C., P. Berry, and A. Smith. 2021. "The climate benefits, co-benefits, and trade-offs of green infrastructure: A systematic literature review." J. Environ. Manage. 291 (Jan): 112583. https://doi.org/10.1016/j.jenvman.2021.112583.
- Chow, V. T., D. R. Maidment, and L. W. Mays. 1998. Applied hydrology. New York: McGraw-Hill.
- City of Phoenix. 2013. Storm water policies and standards. Phoenix: City of Phoenix
- Deb, K., A. Pratap, S. Agarwal, and T. Meyarivan. 2002. "A fast and elitist multiobjective genetic algorithm: NSGA-II." *IEEE Trans. Evol. Com*put. 6 (2): 182–197. https://doi.org/10.1109/4235.996017.
- DelGrosso, Z. L., C. C. Hodges, and R. L. Dymond. 2019. "Identifying key factors for implementation and maintenance of green stormwater infrastructure." J. Sustainable Water Built Environ. 5 (3): 05019002. https:// doi.org/10.1061/JSWBAY.0000878.
- De Neufville, R., and S. Scholtes. 2011. Flexibility in engineering design. Cambridge, MA: MIT Press.
- Dolowitz, D. P., S. Bell, and M. Keeley. 2018. "Retrofitting urban drainage infrastructure: Green or grey?" *Urban Water J.* 15 (1): 83–91. https://doi.org/10.1080/1573062X.2017.1396352.
- Eckart, J., H. Sieker, K. Vairavamoorthy, and K. Alsharif. 2012. "Flexible design of urban drainage systems: Demand led research for Hamburg-Wilhelmsburg." Rev. Environ. Sci. Biotechnol. 11 (1): 5–10. https://doi.org/10.1007/s11157-011-9256-5.
- FCDMC (Flood Control District of Maricopa County). 2014 "Report a flood." Accessed March 1, 2020. https://gis.maricopa.gov/reportaflood/map.html.

- Fletcher, S., M. Lickley, and K. Strzepek. 2019. "Learning about climate change uncertainty enables flexible water infrastructure planning." *Nat. Commun.* 10 (1): 1–11. https://doi.org/10.1038/s41467-019-09677-x.
- Gaffin, S. R., C. Rosenzweig, and A. Y. Y. Kong. 2012. "Adapting to climate change through urban green infrastructure." *Nat. Clim. Change* 2 (10): 704. https://doi.org/10.1038/nclimate1685.
- Gilrein, E. J., T. M. Carvalhaes, S. A. Markolf, M. V. Chester, B. R. Allenby, and M. Garcia. 2019. "Concepts and practices for transforming infrastructure from rigid to adaptable." Sustainable Resilient Infrastruct. 6 (3–4): 1–22. https://doi.org/10.1080/23789689.2019.1599608.
- Golden, H. E., and N. Hoghooghi. 2018. "Green infrastructure and its catchment-scale effects: An emerging science." *WIREs Water* 5 (1): 1–14. https://doi.org/10.1002/wat2.1254.
- Gregoire, B. G., and J. C. Clausen. 2011. "Effect of a modular extensive green roof on stormwater runoff and water quality." *Ecol. Eng.* 37 (6): 963–969. https://doi.org/10.1016/j.ecoleng.2011.02.004.
- Hopkins, K. G., N. B. Grimm, and A. M. York. 2018. "Influence of governance structure on green stormwater infrastructure investment." *Environ. Sci. Policy* 84: 124–133. https://doi.org/10.1016/j.envsci.2018.03 008
- Jain, H., and K. Deb. 2014. "An evolutionary many-objective optimization algorithm using reference-point based nondominated sorting approach, part II: Handling constraints and extending to an adaptive approach." *IEEE Trans. Evol. Comput.* 18 (4): 602–622. https://doi.org/10.1109/TEVC.2013.2281534.
- James, W., L. A. Rossman, and W. R. C. James. 2010. User's guide to SWMM5. 13th ed. Guelph, ON, Canada: CHI Press.
- Kumar, S., R. K. Guntu, A. Agarwal, V. G. K. Villuri, S. Pasupuleti, D. R. Kaushal, A. K. Gosian, and A. Bronstert. 2022. "Multi-objective optimization for stormwater management by green-roofs and infiltration trenches to reduce urban flooding in central Delhi." J. Hydrol. 606 (May): 127455. https://doi.org/10.1016/j.jhydrol.2022.127455.
- Kunkel, K. E., T. R. Karl, M. F. Squires, X. Yin, S. T. Stegall, and D. R. Easterling. 2020. "Precipitation extremes: Trends and relationships with average precipitation and precipitable water in the contiguous United States." J. Appl. Meteorol. Climatol. 59 (1): 125–142. https://doi.org/10.1175/JAMC-D-19-0185.1.
- Leutnant, D., A. Döring, and M. Uhl. 2019. "Swmmr—An R package to interface SWMM." *Urban Water J.* 16 (1): 68–76. https://doi.org/10 .1080/1573062X.2019.1611889.
- Li, J., and S. J. Burian. 2022. "Effects of nonstationarity in urban land cover and rainfall on historical flooding intensity in a semiarid catchment." J. Sustainable Water Built Environ. 8 (2): 1–12. https://doi.org/10.1061 /JSWBAY.0000978.
- Lopez-Cantu, T., and C. Samaras. 2018. "Temporal and spatial evaluation of stormwater engineering standards reveals risks and priorities across the United States." *Environ. Res. Lett.* 13 (7): 074006. https://doi.org/10 .1088/1748-9326/aac696.
- Mailhot, A., and S. Duchesne. 2010. "Design criteria of urban drainage infrastructures under climate change." *J. Water Resour. Plann. Manage*. 136 (2): 201–208. https://doi.org/10.1061/(ASCE)WR.1943-5452 .0000023.
- Manocha, N., and V. Babovic. 2017. "Development and valuation of adaptation pathways for storm water management infrastructure." *Environ. Sci. Policy* 77 (1): 86–97. https://doi.org/10.1016/j.envsci.2017.08.001.
- Markus, M., J. R. Angel, L. Yang, and M. I. Hejazi. 2007. "Changing estimates of design precipitation in northeastern Illinois: Comparison between different sources and sensitivity analysis." *J. Hydrol.* 347 (1–2): 211–222. https://doi.org/10.1016/j.jhydrol.2007.09.024.
- Mentens, J., D. Raes, and M. Hermy. 2006. "Green roofs as a tool for solving the rainwater runoff problem in the urbanized 21st century?" *Landscape Urban Plann*. 77 (3): 217–226. https://doi.org/10.1016/j .landurbplan.2005.02.010.
- Montalto, F. A., C. T. Behr, and Z. Yu. 2011. "Accounting for uncertainty in determining green infrastructure cost-effectiveness." In *Economic in*centives for stormwater control, 246. New York: Island Press.
- MRLC (Multiresolution Land Characteristics). 2021 "Urban imperviousness." Accessed December 1, 2021. https://www.mrlc.gov/data.
- Mwiya, R. M., Z. Zhang, C. Zheng, and C. Wang. 2020. "Comparison of approaches for irrigation scheduling using AquaCrop and NSGA-III

- models under climate uncertainty." *Sustainability (Switzerland)* 12 (18): 7694. https://doi.org/10.3390/su12187694.
- Nieuwenhuijsen, M. J. 2020. "Green infrastructure and health." Ann. Rev. Public Health 42 (Apr): 317–328. https://doi.org/10.1146/annurev-publhealth-090419-102511.
- NOAA and NWS. 2021 "NOAA Atlas 14 point precipitation frequency estimates: KS." Accessed December 1, 2021. https://hdsc.nws.noaa .gov/hdsc/pfds/pfds\_map\_cont.html.
- O'Donnell, E. C., J. E. Lamond, and C. R. Thorne. 2017. "Recognising barriers to implementation of blue-green infrastructure: A Newcastle case study." *Urban Water J.* 14 (9): 964–971. https://doi.org/10.1080/1573062X.2017.1279190.
- Perica, S., S. Pavlovic, M. S. Laurent, C. Trypaluk, D. Unruh, and O. Wilhite. 2018. NOAA Atlas 14 volume 11 version 2, precipitation-frequency Atlas of the United States. Silver Spring, MD: National Weather Service.
- Reed, P. M., D. Hadka, J. D. Herman, J. R. Kasprzyk, and J. B. Kollat. 2013. "Evolutionary multiobjective optimization in water resources: The past, present, and future." In Vol. 51 of Advances in water resources, 438–456. Amsterdam, Netherlands: Elsevier.
- Rossman, L. A. 2006. Storm water management model quality assurance report: Dynamic wave flow routing. Washington, DC: USEPA.
- Rossman, L. A. 2017. Storm water management model reference manual volume II—Hydraulics. Washington, DC: USEPA.
- Rossman, L. A., and W. C. Huber. 2016. Storm water management model reference manual volume III—Water quality. Washington, DC: USEPA.
- Rutgers. 2017 "Maintenance and costs of green infrastructure." Accessed February 10, 2022. https://water.rutgers.edu/Presentations-FixingFlooding /PM\_TractA\_MaintenanceConstructionCosts.pdf.
- Shrestha, A., G. Mascaro, and M. Garcia. 2022. "Effects of stormwater infrastructure data completeness and model resolution on urban flood modeling." J. Hydrol. 607 (Jul): 127498. https://doi.org/10.1016/j .jhydrol.2022.127498.
- Stevenson, S., S. Coats, D. Touma, J. Cole, F. Lehner, J. Fasullo, and B. Otto-Bliesner. 2022. "Twenty-first century hydroclimate: A continually changing baseline, with more frequent extremes." *Proc. Natl. Acad. Sci. U.S.A.* 119 (12): 1–9. https://doi.org/10.1073/pnas.2108124119.
- Swain, D. L., O. E. J. Wing, P. D. Bates, J. M. Done, K. A. Johnson, and D. R. Cameron. 2020. "Increased flood exposure due to climate change

- and population growth in the United States." *Earth's Future* 8 (11): e2020EF001778. https://doi.org/10.1029/2020EF001778.
- Terrascope. 2022. "Implementation and costs." Accessed February 11, 2022. https://terrascope2024.mit.edu/.
- Thorne, C. R., E. C. Lawson, C. Ozawa, S. L. Hamlin, and L. A. Smith. 2018. "Overcoming uncertainty and barriers to adoption of bluegreen infrastructure for urban flood risk management." Supplement, J. Flood Risk Manage. 11 (S2): 1–13. https://doi.org/10.1111/jfr3 12218
- Tsou, C. S. 2013. "nsga2R: Elitist non-dominated sorting genetic algorithm based on R." In *R package version*, 1. Vienna: Comprehensive R Archive Network.
- University of Maryland, and Texas A&M University. 2018. *The growing threat of urban flooding: A national challenge 2018*. College Station, TX: Texas A&M Univ.
- US Census Bureau. n.d. "U.S. and world population clock." Accessed March 20, 2022. https://www.census.gov/popclock/.
- USDA-NRCS (USDA Natural Resources Conservation Service). 2017 "Web soil survey." Accessed December 22, 2021. https://websoilsurvey.sc.egov .usda.gov/App/WebSoilSurvey.aspx.
- USEPA. 2014. Getting to green: Paying for green infrastructure: Financing options and resources for local decision-makers. EPA 842-R-14-005. Washington, DC: USEPA.
- USGS. 2003. Effects of urban development on floods. USGS Fact Sheet FS-076-03. Reston, VA: USGS.
- Webber, J. L., T. D. Fletcher, L. Cunningham, G. Fu, D. Butler, and M. J. Burns. 2020. "Is green infrastructure a viable strategy for managing urban surface water flooding?" *Urban Water J.* 17 (7): 598–608. https://doi.org/10.1080/1573062X.2019.1700286.
- WEF (Water Environment Federation). 2018. Green Infrastructure exceeds expectations. Alexandria, VA: WEF.
- Wickham, H. 2009. "ggplot2." In Applied spatial data analysis with R. New York: Springer.
- Zuniga-Teran, A. A., C. Staddon, L. de Vito, A. K. Gerlak, S. Ward, Y. Schoeman, A. Hart, and G. Booth. 2020. "Challenges of mainstreaming green infrastructure in built environment professions." *J. Environ. Plann. Manage.* 63 (4): 710–732. https://doi.org/10.1080/09640568 .2019.1605890.